Journal of Vibration Engineering & Technologies (2024) 12:633–648
https://doi.org/10.1007/s42417-023-00864-1

ORIGINAL PAPER

Design and Performance Study of Metamaterial with Quasi-zero Stiffness Characteristics Based on Human Body Structure

Hongjie Lu[1] · **Lixin Meng**[1,2] · **Jinkai Wang**[1] · **Yan Wang**[1] · **Lizhong Zhang**[1,2]

Received: 6 October 2022 / Revised: 12 January 2023 / Accepted: 13 January 2023 / Published online: 27 January 2023

Abstract

Purpose The design of a new meta-structure with quasi-zero stiffness (QZS) characteristics based on human body structure not only expands the diversity of quasi-zero stiffness structures but also demonstrates excellent performance in the field of low-frequency vibration damping.

Methods Firstly, a quasi-zero stiffness unit structure combining a horizontal cosine beam and vertical cosine beam is designed based on the human body structure, and multiple unit structures are combined into one meta-structure; secondly, according to the material-structural properties of the unit, a functional relationship is established for the positive stiffness structure using the segmental function method, which is combined with the functional relationship of the negative stiffness structure to obtain the theoretical model of the unit structure and then derives the mechanics of the whole meta-structure behavior of the whole meta-structure. Then, the unit structure model and the meta-structure model are designed and simulated, the static properties of the meta-structure are investigated, and photosensitive resin is chosen as the material in the simulation process. Finally, the transmittance comparison between the meta-structure and the linear vibration isolation structure with different damping coefficients is analyzed by theory, and the vibration isolation performance of the meta-structure is simulated.

Results The static simulation analysis of the meta-structure verifies the theoretical solution of the meta-structure very well. According to the theoretical formulation, different parameters can be input to obtain the quasi-zero stiffness properties of the structure. The quasi-zero stiffness properties of the structure are independent of the inherent material properties. Due to the nonlinear nature of the quasi-zero stiffness unit structure, it not only has a lower peak transmittance, but also a lower resonant frequency and a wider isolation range compared with the linear vibration isolator.

Conclusions The designed quasi-zero stiffness meta-structure is suitable for low-frequency vibration isolation of precision instruments, which can be realized by different materials, and more complex meta-structures can be designed on this basis in the future, which has great potential for application in engineering practice.

Keywords Human body structure · Quasi-zero stiffness · Metamaterials · Vibration isolation performance

Introduction

In many engineering practices, vibration isolation is often a critical issue [1]. A typical example is the optical vibration isolator, which plays an important role in the stability of the optical view axis and the accuracy of communication. The ideal optical vibration isolator achieves good vibration isolation in both the low and wide frequency ranges. To meet these different needs, there are many types of vibration isolators available, ranging from conventional rubber dampers to passive spring isolators to active vibration isolators [2–5]. Typically passive spring isolators are the most used and are known for their high reliability, ease of implementation, and

✉ Lixin Meng
mengcust@163.com

[1] College of Mechanical and Electrical Engineering, Changchun University of Science and Technology, Changchun 130022, China

[2] Key Laboratory of Air-to-Ground Laser Communication for National Defense, Changchun University of Science and Technology, Changchun 130022, China

low development cost, but may not be effective for low or wide-frequency isolation [6–8].

Smaller resonant frequencies are often expected in the design of vibration isolators to achieve better isolation performance. However, a smaller resonant frequency implies a lower stiffness (or heavier mass), resulting in the generation of a lower load capacity (or a bulky system). Therefore, a large number of scholars have investigated some nonlinear isolation methods that possess high static stiffness, while exhibiting good isolation performance in the low-frequency band [9, 10].

In 1957, Molyneux proposed a three-spring QZS isolator [11], which is considered to be the earliest QZS isolation device, and the high static-low dynamic stiffness of this device opened up a new research direction for low-frequency isolation vibration. In the past 10 years, the theoretical analysis, design, and experimental research of QZS vibration isolators have been widely reported. The QZS structure is mainly composed of two parts: positive and negative stiffness. Different types of quasi-zero stiffness isolators can be constructed depending on the different composition structures of negative stiffness (e.g., inclined springs, horizontal springs, cam springs, roller springs, magnetic springs, and Eulerian bending beams) and positive stiffness [12–16]. Cao et al. studied the transition from smooth to discontinuous dynamics of a three-spring system, which in the smooth region bears a clear resemblance to the Duffing oscillator, exhibiting standard dynamics controlled by a hyperbolic structure associated with the fixed state of the double trap. However, in the discontinuity limit, the dynamics are quite different from the standard limit [17]. Zhu et al. proposed a generalized inverse method for structural construction, which showed that elliptical trajectory tracking of the designed model is a sufficient condition for satisfying the zero stiffness property, and that the unique geometry of the zero-stiffness system provides new inspiration for the resonance-free design of metamaterial cells, and that the inverse method can even enable the more targeted application of the design to arbitrarily complex dynamical requirements [18]. Hao et al. proposed a dynamical model for a single-degree-of-freedom spring-mass system, which can be used as a reference for nonlinear support systems and stable-quasi-zero stiffness (SQZS) vibration isolation systems for large aircraft ground vibration test (GVT) [19]. In addition, the dynamics analysis of the perturbed system near the optimized parameters reveals complex behaviors such as KAM structure, multiplicative period, chaotic crisis, multi-solution coexistence, intermittent chaos, and chaotic saddle, which provide a basis for better understanding of the complex dynamics of SQZS nonlinear systems. Sun et al. designed a vibration isolation platform with an n-layer scissor truss structure to achieve QZS characteristics by controlling different structural parameters to better achieve superior vibration isolation performance [20]. Zhou et al. proposed a new passive asymmetric quasi-zero stiffness vibration isolator (AQZS-VI) consisting of a combination of two linear springs, cantilever plate springs and L-shaped rods (CPS-LSL). The proposed AQZS-VI has superior vibration isolation performance with lower vibration isolation onset frequency and better performance of displacement transfer capability than the linear model [21]. Chang et al. proposed a quasi-zero stiffness dynamic damper (QZS DVA) for the ultra-low-frequency absorption method. The conceptual design of the QZS DVA was carried out using a simple inclined spring model. The dynamic behavior of the QZS DVA system under harmonic excitation and random pulses was investigated and verified by numerical analysis and experiments [22]. Ye et al. designed an integrated flat-rotating rotating QZS isolator using a cam-roller mechanism capable of providing high static-low dynamic stiffness in both directions simultaneously, and studied its nonlinear dynamic response by numerical and theoretical methods [23]. Xiong et al. designed a quasi-zero stiffness vibration isolation system with an additional X-shaped structure (X-QZS) by connecting the X-shaped structure to the platform. The designed X-QZS system has a wide QZS interval, small instability interval, low jump frequency, and high load carrying capacity [24]. Hao proposed a single- degree-of-freedom geometrically nonlinear oscillator with stable quasi-zero stiffness (SQZS), modeled to include a set total mass covering an isolated object and a pair of horizontal springs that provide negative stiffness parallel to a vertical linear spring to carry the load. Frequency band parameter optimization was performed using an extended averaging method to obtain the frequency response characteristics of the model. In addition, numerical simulations were performed to detect complex dynamical phenomena of periodic, chaotic motion [25]. Yan proposed a lever-type quasi-zero stiffness vibration isolator (L-QZS-VI), where the QZS characteristic is achieved by a magnetic spring. Eddy current damping (ECD) is used to eliminate the jump phenomenon. A theoretical model of L-QZS-VI with ECD is established, and the effects of the tip mass of the lever, the lever ratio, the nonlinear stiffness of the magnetic spring, and the excitation amplitude on the vibration isolation performance of L-QZS-VI are analyzed numerically and experimentally [26]. Lu et al. investigated a coupled quasi-zero stiffness (QZS) vibration isolator for axially loaded beams to improve the effectiveness of low-frequency isolation. A QZS contains two magnetic rings with negative stiffness and a coil spring with positive stiffness, which have high static stiffness to resolve the structural instability. Analytical and numerical results show that the axially loaded beam of the parallel-coupled quasi-zero isolation system has a more significant suppression of power reduction at low frequencies [27]. Hao investigated the nonlinear energy transfer in an arbitrary boundary flexible plate coupled by a high static low dynamic stiffness (HSLDS) isolator. The nonlinear coupling dynamics equations are derived using the Lagrangian method, and the modified Fourier series method and Rayleigh–Ritz method give the modal coefficients of the arbitrary boundary flexible plate with nonlinear isolators. In addition, the analytical results of the modal shape of the flexible plate are verified by the finite element simulation used in this paper, and the isolation performance of the nonlinear vibrator supported on the flexible plate is experimentally verified [28]. Most researchers have focused on quasi-zero stiffness structures for large equipment, and less on quasi-zero stiffness vibration isolators for precision instruments.

The term "metamaterials" is commonly used to describe artificial composite materials consisting of periodic or random arrangements of artificial subwavelength structures. Metamaterials mainly include electromagnetic metamaterials [29], optical metamaterials [30–33], acoustic metamaterials [34], and mechanical metamaterials [35]. Mechanical metamaterials achieve idiosyncratic mechanical properties through the internal design of the unit structure. Mechanical metamaterials are not only a complement to conventional natural materials, but also they have gradually become the protagonists in the field of new materials, endowed with richer functional properties, including reconfigurability, programmability, self-determination, and mechanical operations. In the future, the functional properties of natural materials will gradually fade away, and will more often be used as components of functional metamaterials in the form of raw materials. This paper focuses on vibration isolation research, mainly on mechanical metamaterials to manipulate the overall equivalent stiffness of the structure. In recent years, the combination of quasi-zero stiffness properties and mechanical metamaterials has provided a new way for the development of vibration isolation of small precision instruments.

Cai et al. proposed a new metamaterial plate structure with quasi-zero stiffness (QZS) resonators, which were theoretically derived, numerically simulated, and experimentally investigated for wave propagation characteristics and showed excellent attenuation in the ultra-low-frequency band gap [36]. Li et al. designed a bistable hybrid symmetric laminate (BHSL) as a negative stiffness element to design quasi-zero stiffness vibration isolators. The theoretical model and finite element model were validated from the static and dynamic analysis [37]. Lin has developed a novel two-dimensional (2D) locally resonant (LR) metamaterial with quasi-zero stiffness (QZS) properties in both horizontal and vertical directions. The anisotropy of the precompression along the horizontal and vertical directions can be exploited so that the complete band gap covers different frequency ranges, providing a way to achieve a complete band gap at low frequencies, independent of the direction of incidence of the in-plane waves [38]. Ye proposed a truss-spring-based stack Miura-ori (TS-SMO) structure to provide the required stiffness for high static—low dynamic requirements. A QZS vibration isolator is then designed based on specific parameters. The static performance of the system was verified by the force–displacement response. The dynamic analysis using the harmonic balance method (HBM) and numerical simulation was used to derive the displacement transmittance, and the isolation performance under variable viscous damping was also discussed to examine the effect of system damping [39]. Fan et al. designed a meta-structure combining the penetration behavior of a sinusoidal beam and the bending dominant support of two semicircular arches, which in turn achieved quasi-zero stiffness properties for each cell, and analyzed the static and dynamic properties of the meta-structure. The results show that the meta-structure can achieve good quasi-zero stiffness with excellent vibration isolation performance by designing the cells correctly [40]. The combination of quasi-zero stiffness and metamaterials offers a new approach to low-frequency vibration reduction that has an important role in future engineering.

The human body encounters several types of whole-body vibration in daily life: the more common ones are walking, running and jumping [41].This is when the human body acts as a damper to prevent damage to the brain from vibrations and shocks [42]. The resonant frequency of the human body varies for different body postures [43]. Especially, when people stand with their knees bent, the peak of the transmission rate is even below 3 Hz. At the same time, the human body is able to attenuate frequencies of 20 Hz and above [44].

The excellent vibration isolation characteristics of the human body discussed above provide a novel vibration isolation structure design for this study, which has the potential to achieve very good ultra-low-frequency vibration isolation and excellent vibration isolation performance over a wide frequency range. In this study, a vibration-damping structure based on human body structure is proposed as shown in Fig. 1 and Fig. 2.The new structure consists of two parts: a double vertical cosine beam structure to simulate the human bent leg, and a horizontal cosine beam structure to imitate the human upper body arm. The layout of the proposed vibration-damping system is shown in Fig. 2.

In this paper, a new meta-structure with quasi-zero dynamic stiffness is designed based on human foundation structure, and its characteristics in vibration isolation applications are investigated by combining theoretical analysis and finite element simulation. In Section "Human-inspired vibration isolation structure model", a meta-structure consisting of several cells is designed and the mechanical behavior with quasi-zero stiffness is derived. In Section "Static properties of the meta-structure", the static properties of the structure under uniaxial compression are investigated through simulations. Section "Dynamics analysis" studies the dynamic characteristics and vibration isolation performance of the meta-structure. Section "Conclusion" gives the

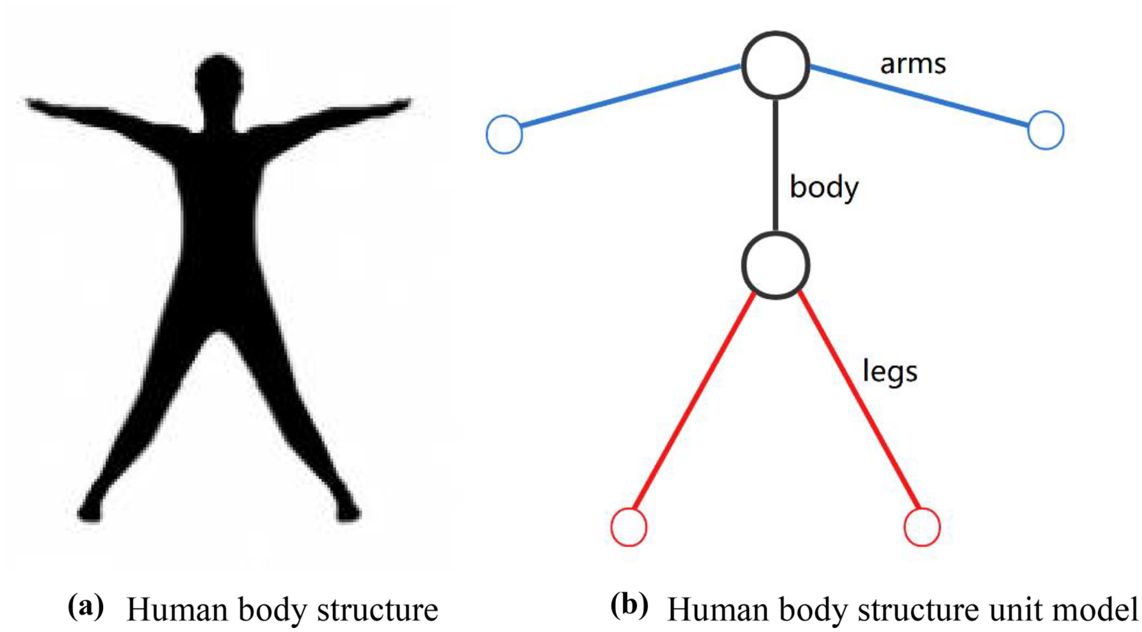

Fig. 1 Human body structure diagram and unit model

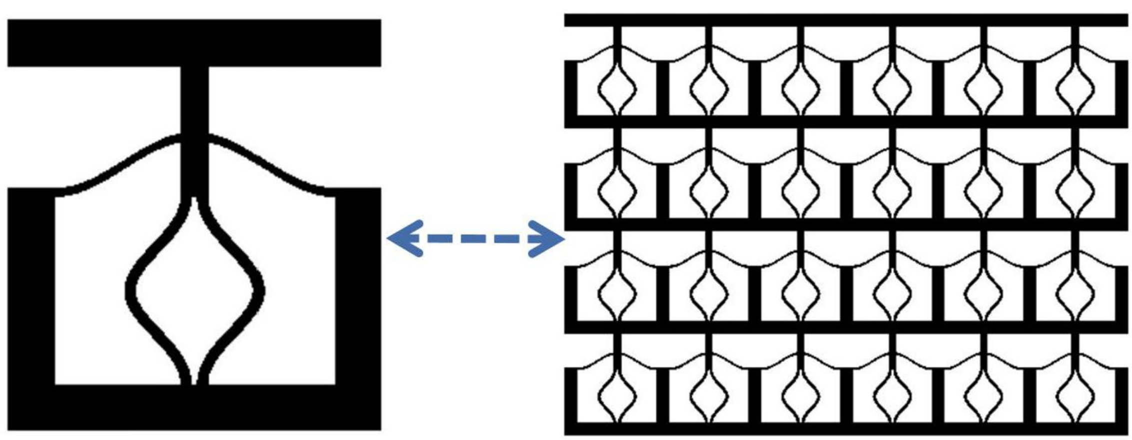

Fig. 2 Quasi-zero stiffness unit cell and meta-structure for human-like structural design

conclusion. The structure not only extends the diversity of quasi-zero stiffness structures, but also has great potential for application in the field of low-frequency vibration isolation of small continuous structures.

Human-Inspired Vibration Isolation Structure Model

To facilitate discussion and interpretation, the quasi-zero stiffness structure in Fig. 2 is re-arranged as Fig. 3, and the structural parameters are clearly stated.

As shown in Fig. 3, the unit structure consists of horizontal and vertical cosine beams and stiffer stiffening walls. Since the horizontal cosine beam provides negative stiffness characteristics and the vertical cosine beam provides positive stiffness characteristics, the quasi-zero stiffness characteristics are produced by the proper arrangement of the two structures. As shown in Fig. 3, the shape of the horizontal cosine beam is given by $y = h_1/2\left[1 - \cos\left(2\pi x/l_1\right)\right]$. The length is l_1, the depth is b_1, the thickness is t_1, and the amplitude is t_1. The shape of the vertical cosine beam is then given by $x = h_2/2\left[1 - \cos\left(2\pi y/l_2\right)\right]$. The length is l_2, the depth is b_2, the thickness is t_2, and the amplitude is h_2. The cosine beam is connected by a stiffening wall of thickness t. By a

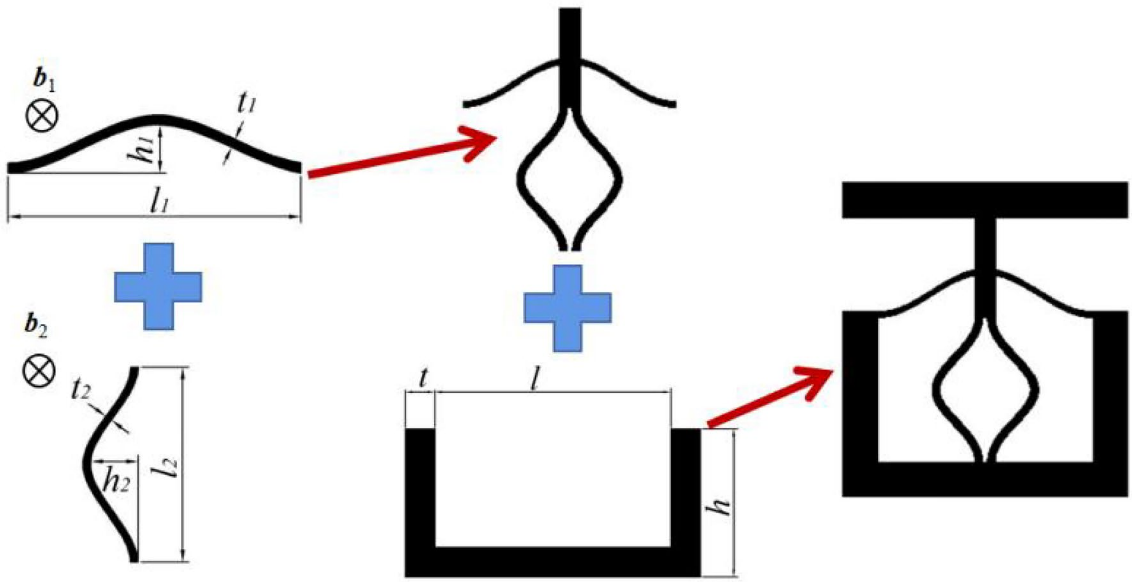

Fig. 3 Quasi-zero stiffness structural model of human-like structural design

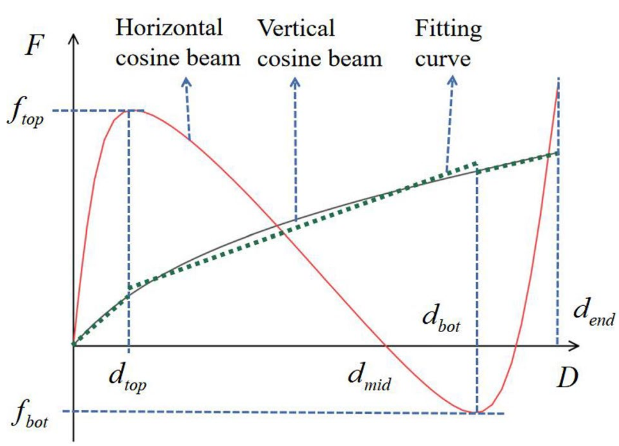

Fig. 4 Force–displacement curves of horizontal cosine beam and vertical cosine beam

reasonable arrangement of negative and positive stiffnesses, the unit will have quasi-zero stiffness.

Mechanical Model of the Unit Structure

According to Qiu et al. [45], when the parameters of the cosine beam satisfy $h_1/t_1 \geq 6$, its force–displacement curve can be approximated by three connected straight lines, as shown in Fig. 4.The corresponding parameters in the force–displacement curve are shown in Eq. 1, where E is the Young's modulus of the material and I_1 is the moment of inertia of the beam.

$$f_{top} \approx 740\frac{EI_1h_1}{l_1^3} \quad f_{bot} \approx 370\frac{EI_1h_1}{l_1^3} \quad d_{mid} = \frac{4}{3}h_1 \tag{1}$$

$$d_{top} = 0.16h_1 \ d_{bot} = 1.92h_1 \ d_{end} = 1.99h_1. \tag{2}$$

Assuming that the transverse displacement component is constant along the thickness direction, the stiffness of the cosine beam in three different stages is shown in Eq. 3

$$k_{a1} \approx \frac{4625EI_1}{l_1^3} \quad k_{a2} \approx -\frac{13875EI_1}{22l_1^3} \quad k_{a1} \approx \frac{37000EI_1}{7l_1^3}. \tag{3}$$

For the vertical cosine beam, which mainly provides positive stiffness, the force–displacement curve under vertical displacement is shown in Fig. 4. The overall stiffness of the beam shows a nonlinear relationship, but when compared with a horizontal cosine beam that provides negative stiffness, the positive stiffness cosine beam can be divided into three stages with approximately linear force and displacement curves in each stage, allowing the stiffness to have constant values in different stages.

As shown in Fig. 5, according to beam theory, the stiffness will be proportional to the Young's modulus E of the material, the moment of inertia I_2 of the beam and the inverse of the cube of the vertical cosine beam length l_2.And the segmented function relationship is presented with the cut-off point of $0.16h_2$ and $1.92h_2$.The method of segmented functions used in this paper can be regarded as a special form of calculus, using a straight line approximation to fit the curve. In this paper the force and displacement curves

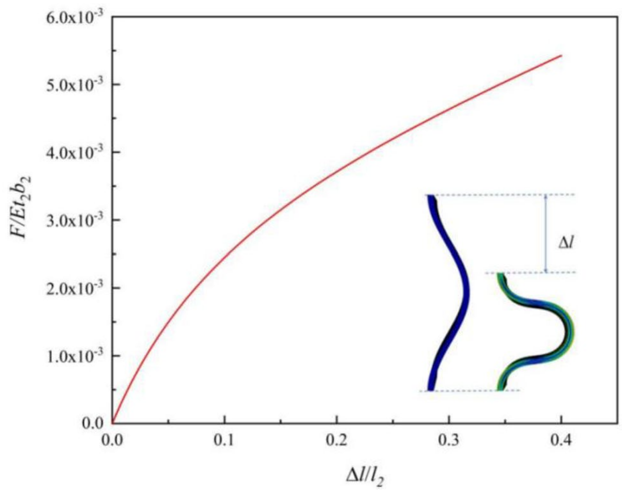

Fig. 5 Dimensionless force–displacement curve of vertical cosine beam

for negative stiffness are divided into three segments, so the positive stiffness is also divided into three segments. Different analyses can be performed in subsequent applications according to their own conditions. In this paper, the variation of stiffness and displacement of the vertical cosine beam can be written as:

$$k_b = \begin{cases} \alpha \frac{EI_2}{l_2^3} & \Delta l < 0.16h_1 \\ \beta \frac{EI_2}{l_2^3} & 0.16h_1 < \Delta l < 1.92h_1 \\ \gamma \frac{EI_2}{l_2^3} & 1.92h_1 < \Delta l < 1.99h_1 \end{cases}, \tag{4}$$

where α, β, γ are three dimensionless coefficients. It should be noted that the dimensionless coefficients corresponding to the different cross sections can be obtained by elastic analysis [46] and the finite element method. To reflect the deformation response of the vertical cosine beam and to ensure that it is always in an elastic state when displaying quasi-zero stiffness characteristics, this paper uses ABAQUS for finite element analysis. The cosine beam is modeled with a solid unit of linear elastic material C3D20R, and the vertical end part shift is $0.4 \times l_2$. Multiple simulations were performed for cosine beams of different thicknesses, and dimensionless coefficients α, β, γ could be obtained by fitting the curves to the stiffness–thickness relationship. In this paper, we take the vertical cosine beam with the parameter $t_2/l_2 = 0.05$ as an example. The simulation results and dimensionless force–displacement curves of the cosine beam under the action of vertical displacement are shown in Fig. 5. Since the force and displacement curves of the horizontal cosine beam are mainly divided into three segments, the vertical cosine beam force displacement curve is also divided into three segments and approximated as three straight lines, and

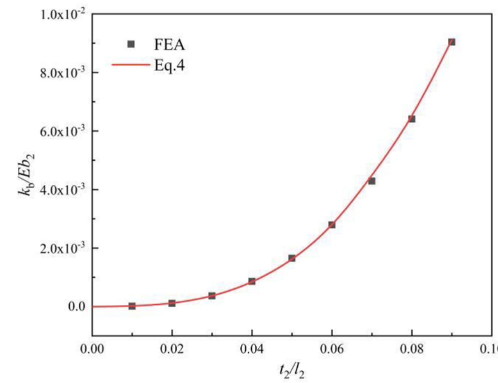

(a) Fitting curve of the first segment stiffness and FEA results

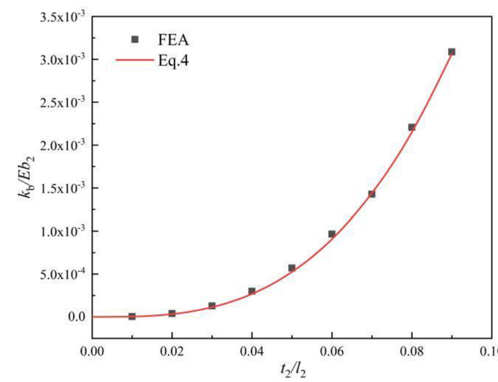

(b) Fitting curve of the second segment stiffness and FEA results

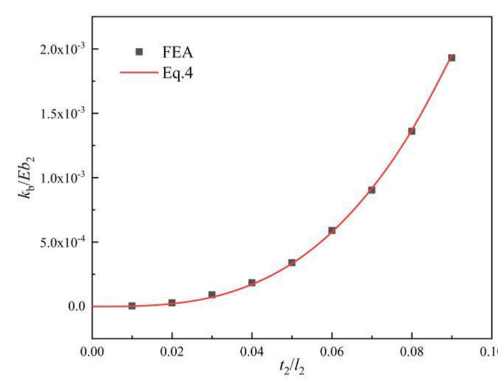

(c) Fitting curves of the third segment stiffness and FEA results

Fig. 6 Fitting curve of vertical cosine beam stiffness and comparison results of finite element analysis

the stiffness of the cosine beam can be found as $k_b = F/\Delta L$. The resulting finite element result for the stiffness of cosine beams with different thicknesses and dimensionless stiffness k_b/Eb_2 under parameter t_2/l_2 are shown in Fig. 6.

The triple fitted curves agree well with the finite element results, and the dimensionless coefficients $\alpha = 150.25$, $\beta = 50.44$ and $\gamma = 32.44$ are obtained.

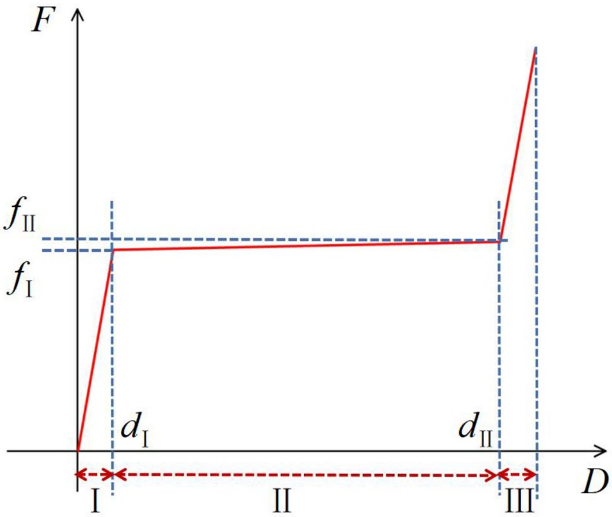

Fig. 7 Force–displacement curve of the unit structure

Considering that the horizontal cosine beam and the vertical cosine beam are arranged in parallel, the stiffness of the unit under vertical displacement is the sum of the respective stiffnesses. Therefore, the force–displacement curve of the cell can also be represented by three connected straight lines to obtain quasi-zero stiffness in region II, as shown in Fig. 7. The expression for the stiffness of the unit can be as follows:

$$k_1 = k_{a1} + 2k_{b1}\ k_2 = k_{a2} + 2k_{b2}$$

$$k_3 = k_{a3} + 2k_{b3}. \tag{5}$$

By correctly selecting the parameters of the horizontal and vertical cosine beams, it is possible to design the stiffness of different regions and obtain the appropriate static stiffness to support the isolation weight, as well as the quasi-zero dynamic stiffness to ensure the vibration isolation performance.

Static Properties of the Meta-structure

Unit Structure Design

In this paper, three different cell structuresU_1, U_2 and U_3 are designed, as shown in Fig. 8, and only the parameters t_2 of each cell are different, the rest of the parameters are the same. $l_1 = l = 60\ mm$, $t_1 = 2\ mm$, $h_1 = 12\ mm$, $b_1 = 10\ mm$, $l_2 = 40\ mm$ $h_2 = 12\ mm$, $b_2 = 10\ mm$, $t = 10\ mm$, $h = 50\ mm$. By theoretical solution, the unit structure reaches quasi-zero stiffness at $t_2 = 2.45\ mm$, and two cases of $t_2 = 2\ mm$ and $3\ mm$ are designed, respectively, with three different structures representing positive stiffness, negative stiffness and

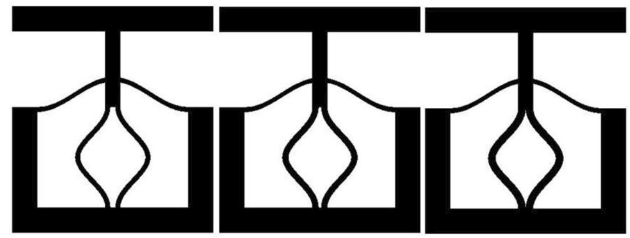

Fig. 8 Unit structure model (U_1, U_2, U_3)

quasi-zero stiffness. Two samples of meta-structures with different parameters were also designed to study their static properties. The specific parameters of the meta-structure are shown in Table 1. A photosensitive resin [47] was used as a constituent material for the preparation of the samples. Young's modulus of photosensitive resin was $E = 1.4Gpa$.

Numerical Simulation

Finite element analysis of the static properties of the meta-structure was carried out using finite element software. The meta-structure is modeled with a tetrahedral mesh, ten-node quadratic tetrahedral cells (C3D10), and mesh sensitivity testing is performed to ensure accuracy. Due to the large deformation behavior of the structure, geometric nonlinearities need to be taken into account. In order to simulate the actual behavior of the meta-structure under compression, all six degrees of freedom (three translations and three rotations) are constrained on the bottom surface of the structure, and the top surface of the structure is coupled to a reference point where all five degrees of freedom are constrained, except for the displacement in the compression direction. In the static generic step, a specified displacement is applied to the reference point to simulate the compression process of the structure. It should be clear that in the theoretical analysis, the stiffened walls of the structure should be rigid. This means that the left and right sides of the structure are constrained and only translations in the displacement direction are allowed. However, in the actual compression test, the left and right edges of the structure were free, causing the stiffened walls to deform. Therefore, these two different boundary conditions are considered simultaneously in the numerical simulation, as shown in Fig. 9. In the theoretical analysis simulation, the left and right edge of the structure are set as constrained boundaries (CB).

As an example, the cell structure U_2 shows the behavior of the cell under different vertical displacements, as shown in Fig. 10. The reaction forces of the U_1, U_2 and U_3 unit structures under vertical displacement are shown in Fig. 11. The results show that the cell can exhibit positive, quasi-zero and negative stiffness characteristics in region II through a reasonable design. For the unit structure U_1, the absolute

Table 1 Meta-structural parameters

Meta-structure	Number of arrangements	Structure parameters										
		l_1	t_1	h_1	b_1	l_2	t_2	h_2	b_2	h	t	l
S_1	3 rows and 4 columns	50	1.0	6.0	10	30	1.106	6.0	10	40	10	50
S_2	4 rows and 5 columns	30	0.5	4.0	5.0	18	0.58	4.0	5.0	23	5.0	30

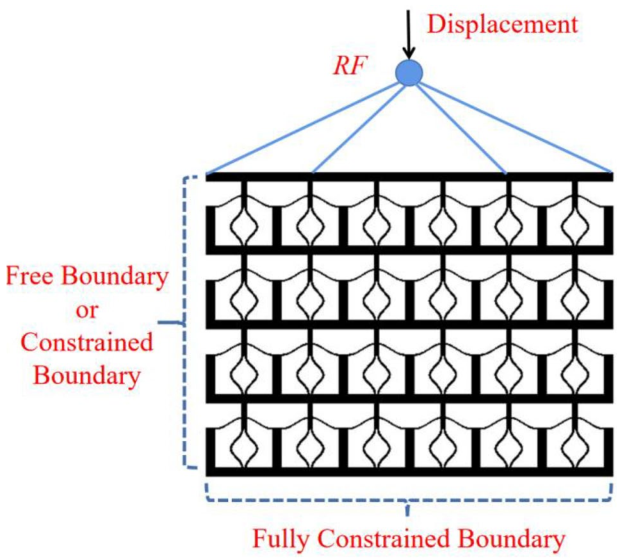

Fig. 9 Finite element model of the meta-structure

value of the positive stiffness $2k_{b2}$ of the vertical cosine beam is smaller than the absolute value of the negative stiffness k_{a2} of the horizontal cosine beam. From Eq. 5, the unit U_1 is a negative stiffness of $k_2 < 0$. Similarly, for samples U_2 and U_3, the absolute value of the positive stiffness $2k_{b2}$ is almost equal to or greater than the negative stiffness k_{a2}. The $k_2 \rightarrow 0$ quasi-zero stiffness and the positive stiffness with $k_2 > 0$ are obtained for U_2 and U_3, respectively. The results show that the quasi-zero stiffness properties of the structure are determined due to the internal periodic cell structure rather than due by the inherent properties of the material.

By studying the response of the two meta-structures S_1 and S_2 under vertical displacement conditions for the structure under FB and CB conditions, the simulation results are shown in Figs. 12 and 13. The results show that the deformation of the horizontal cosine beam exhibits fast passage and the deformation of the vertical cosine beam is dominated by bending in each cell under FB and CB conditions. For the internal unit of the meta-structure, the horizontal cosine beam undergoes classical symmetric buckling behavior during compression. And for the left and right edges of the meta-structure under FB conditions, the buckling behavior of the horizontal cosine beam is asymmetric. This phenomenon will change the horizontal cosine beam to be asymmetric. This phenomenon will change the horizontal cosine beam stiffness properties and thus adversely affect the quasi-zero stiffness properties of the meta-structure. Since the asymmetric buckling occurs only at the edges of the structure, the adverse effect on the quasi-zero stiffness performance of the meta-structure will gradually decrease with the gradual increase in the number of cells.

The vertical displacements and reaction forces of the meta-structure in the numerical simulation were recorded and compared with the theoretical results, as shown in Fig. 14 and Fig. 15. From the theoretical and simulation results, it can be seen that in the initial stage, the reaction force of the meta-structure increases rapidly with the increase of the compression displacement. This is because, in the initial stage, both the horizontal cosine beam and the vertical cosine beam of each unit structure provide positive stiffness. When the compression displacement exceeds the initial stage, the horizontal cosine beam of the unit structure exhibits negative stiffness, which cancels with the positive stiffness of the vertical cosine beam, causing the positive stiffness of the elemental structure to drop to quasi-zero stiffness. When the vertical displacement exceeds a certain value, the stiffness of the horizontal cosine beam changes back to positive stiffness, and each unit structure provides positive stiffness again. With the gradual increase of the compression displacement, the meta-structure will experience the transition from quasi-zero stiffness to positive stiffness.

Comparing the theoretical solution and simulation results of CB boundary conditions in Fig. 13 and Fig. 15, it can be found that both the theoretical solution and simulation results show good agreement, except for the region of the two transition points between positive and quasi-zero stiffness. This is because large deformations and nonlinear responses are considered in the simulation analysis, while the theoretical model is based on the assumption of small deformations. Therefore, the simulation analysis results in a nonlinear force–displacement curve and the theoretical solution results in a linear one. As h_1/t_1 of the cosine beam increases, the nonlinear effect gradually decreases, and the theoretical and simulation results become closer and closer. Even if there is a discrepancy between the theoretical and simulation results in the transition region, the theoretical solution accurately reflects the quasi-zero stiffness properties of the meta-structure. It is verified that the theoretical model in this paper can effectively evaluate the mechanical

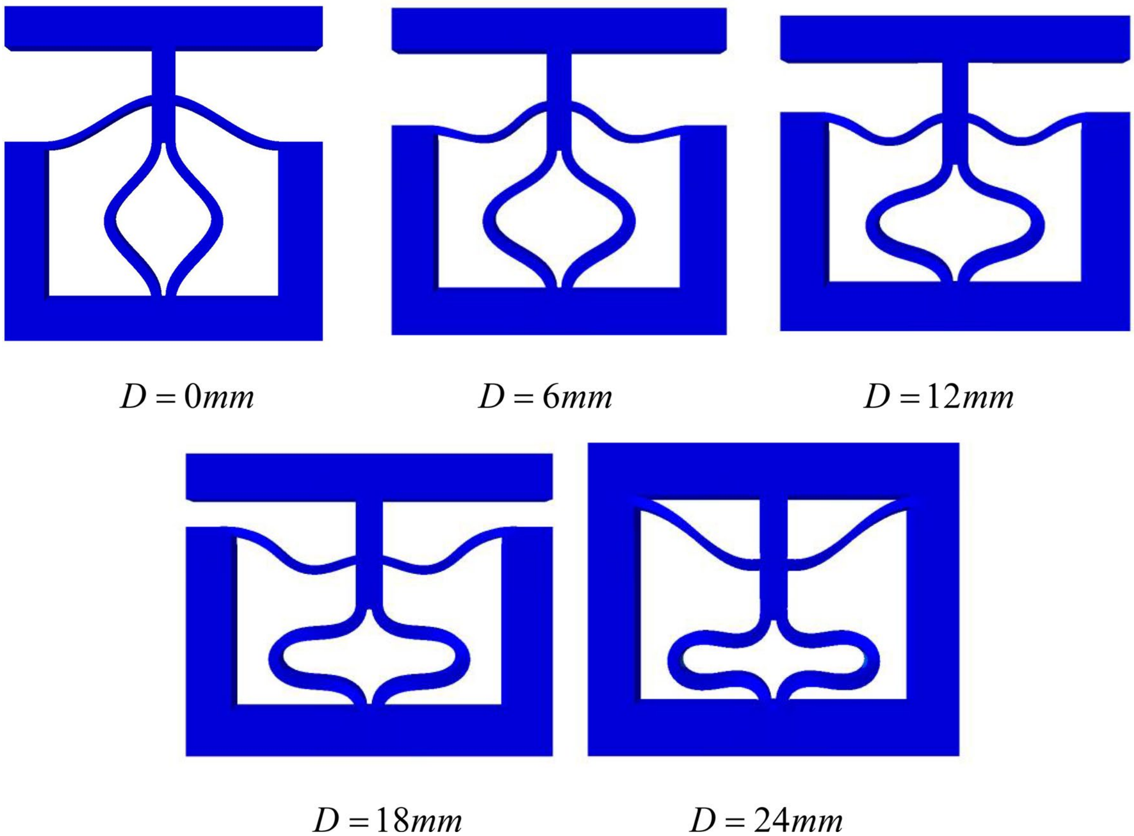

Fig. 10 Behavior of the unitary structure under vertical displacement

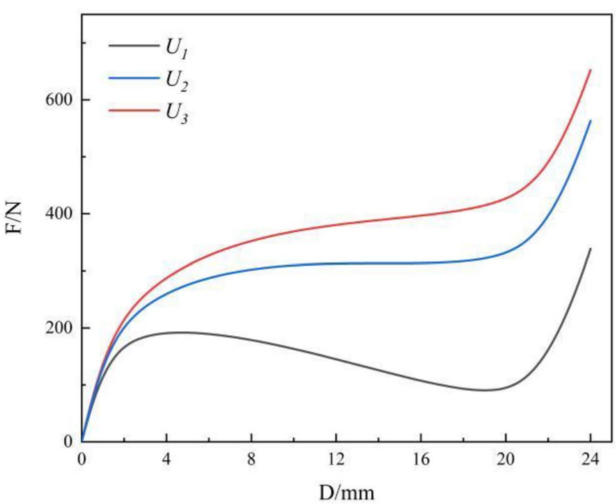

Fig. 11 Force–displacement curves of unitary structures U_1, U_2 and U_3

properties of quasi-zero stiffness element structures when designing quasi-zero stiffness element structures.

The quasi-zero stiffness properties of the simulated results in Figs. 13 and 15 are slightly weakened in the FB boundary condition compared to the theoretical and simulated results in the CB boundary condition, mainly due to the asymmetric buckling of the horizontal cosine beam of the boundary cell caused by the absence of constraints on the left and right edges of the structure. However, as mentioned before, the influence of the boundary conditions decreases as the number of unit structures gradually increases.

Dynamics Analysis

Power Transmission Characteristics

Based on the static properties, the vibration isolation performance of the designed meta-structure was investigated. The results of the static force characteristics analysis show that the mechanical behavior of the meta-structure under vertical displacement contains three regions, quasi-zero stiffness region II and two approximately linear stiffness regions I and III. For objects placed on the meta-structure isolated from vibration, their weight is mainly supported by the approximate linear stiffness of region I. When the vibration excitation acts on the meta-structure, the object will rely on the quasi-zero stiffness of region II for

Fig. 12 Comparison of response under FB and CB structures obtained by simulation of S_1

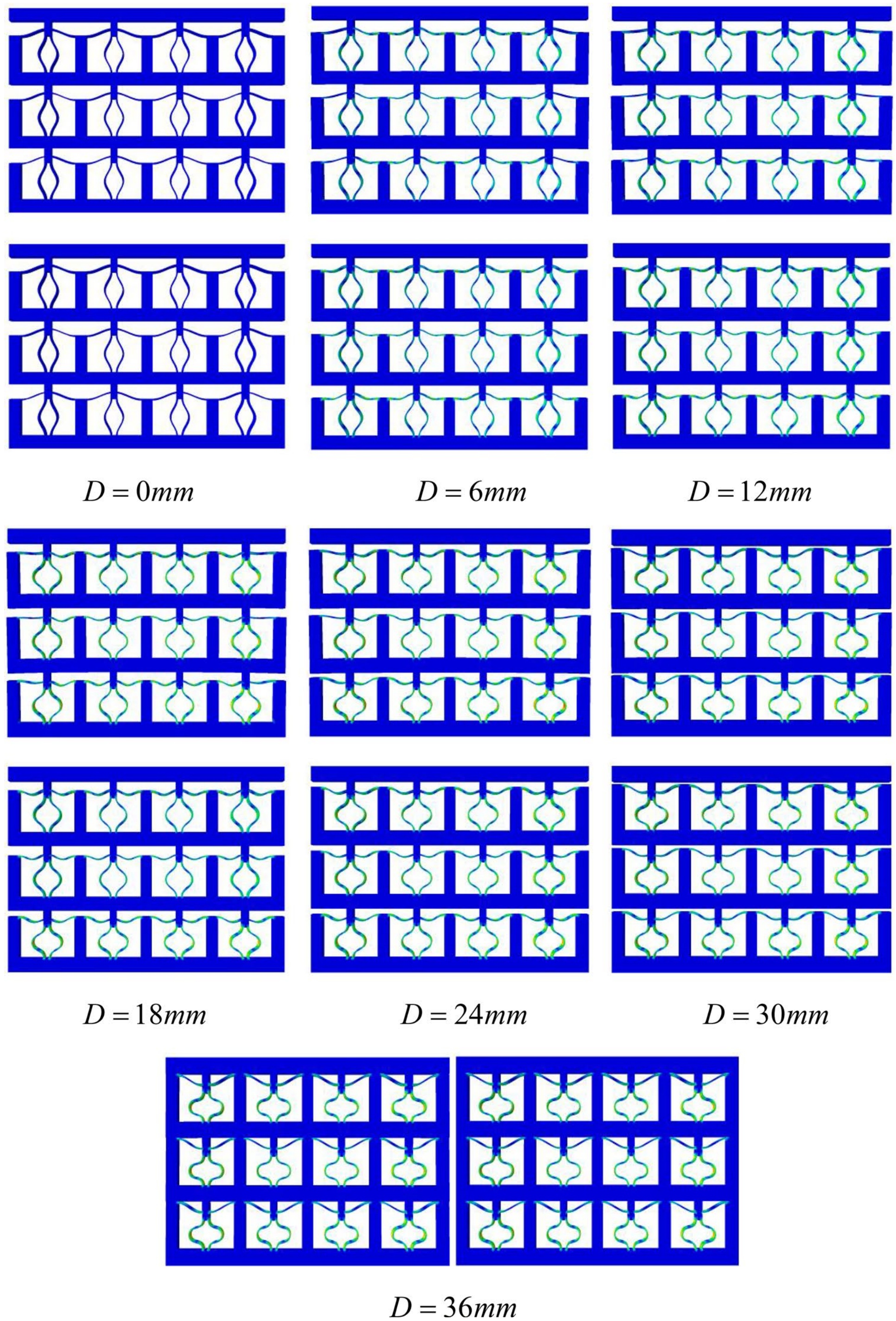

effective isolation. In order to study the vibration isolation characteristics of the meta-structure, the dynamic characteristics of models S_1 and S_2 were investigated. Assume that the upper surface of the specimen supports an object and the lower surface is excited by displacement-controlled vibration. The object with mass M is located in the meta-structure II region, and the gravitational force provided by the object with mass M is replaced by the corresponding concentrated force in the simulation calculation.

The most important index to describe the performance of an isolator is transmissibility. Assume that the bottom of the meta-structure is subjected to displacement-controlled vibration excitation $Z = Z_0 \sin \omega t$, where Z_0 is the vibration amplitude and is the ω vibration frequency. In the case of

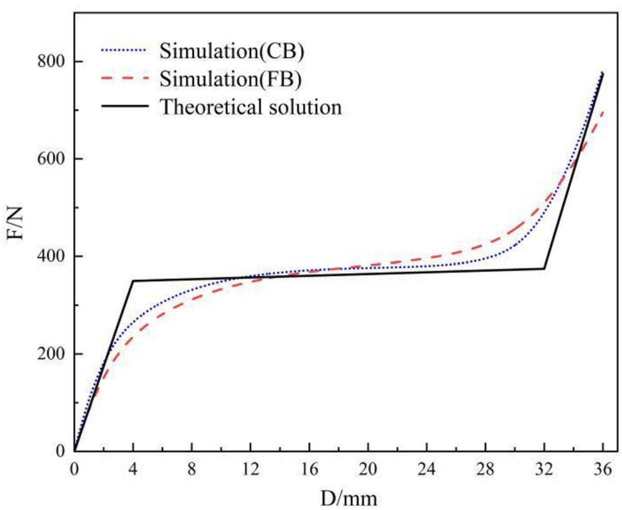

Fig. 13 Force–displacement curves obtained from the theoretical solution and simulation of S_1

meta-structure isolation, the vibration amplitude Z_1 at the top of the meta-structure can be obtained. The transfer rate was defined as $T = Z_1/Z_0$ to evaluate the vibration isolation performance of the meta-structure. For a conventional linear spring isolator, the transfer rate equation can be derived as:

$$T = \sqrt{\frac{K^2 + c^2\omega^2}{(K - M\omega^2)^2 + c^2\omega^2}}, \quad (6)$$

where K is the linear stiffness of the spring and c is the damping of the spring material. In fact, the quasi-zero stiffness is also approximately linear, having a rather small stiffness K_2.Thus, the transfer rate of the meta-structure can be obtained by Eq. 6, where K is replaced by K_2.Since the weight of the object in the meta-structure is mainly supported by K_1, an equivalent linear spring isolator with stiffness K_1 is introduced to verify the vibration isolation performance of the proposed meta-structure with QZS characteristics. Comparison with an equivalent linear vibration isolator is an effective method to verify the vibration isolation performance of the newly designed QZS structure [48, 49].The transfer rate of the linear spring isolator can also be obtained by replacing K by K_1 in Eq. 6.

Comparison of QZS Element Structure and Linear Isolator

Figures 16 and 17 plot the transmittance of the linear spring isolator and the QZS structural models S_1 and S_2. All transmittance results are expressed in dB, i.e., 20log10T. The vibration excitation frequency ratio is expressed in dimensionless form as $\Omega = \omega/\omega_n$, where $\omega_n = \sqrt{K_1/M}$.The dimensionless damping coefficient of the meta-structure is defined as $\xi = c/2\sqrt{K_1 M}$. As shown in Fig. 16 and Fig. 17, for linear isolators, the effective isolation range should meet $\Omega > 1.414$.And for the proposed QZS meta-structural models S_1 and S_2, the effective isolation ranges satisfy $\Omega > 0.116$ and $\Omega > 0.114$, respectively. Compared with the linear vibration isolator, the proposed QZS element structure has a wider effective vibration isolation range and can be effectively isolated at lower vibration frequencies.

In addition to the wide effective isolation range, the QZS meta-structure also has a low transmittance.

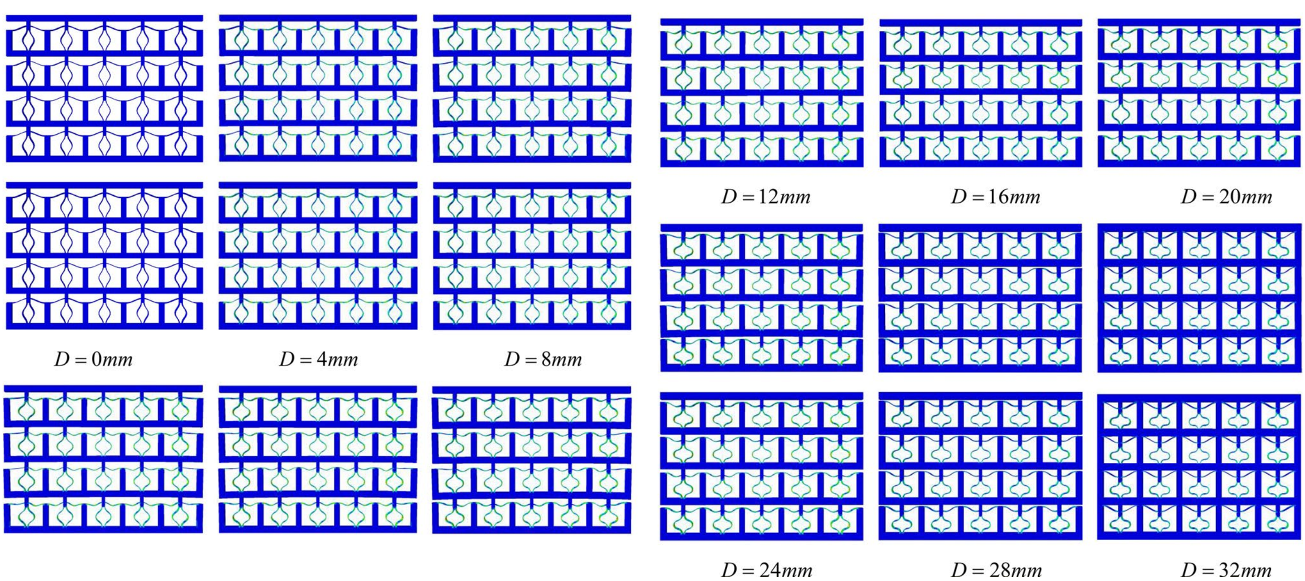

Fig. 14 Comparison of response under FB and CB structures obtained by simulation of S_2

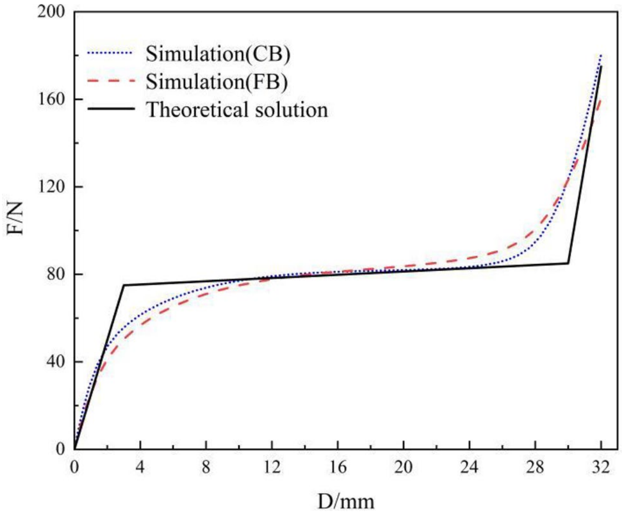

Fig. 15 Force–displacement curves obtained from the theoretical solution and simulation of S_2

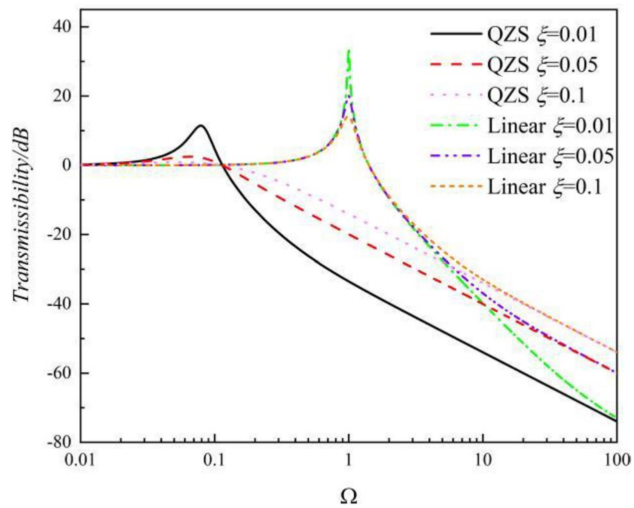

Fig. 17 Transmittance of linear vibration isolator and S_2 structure

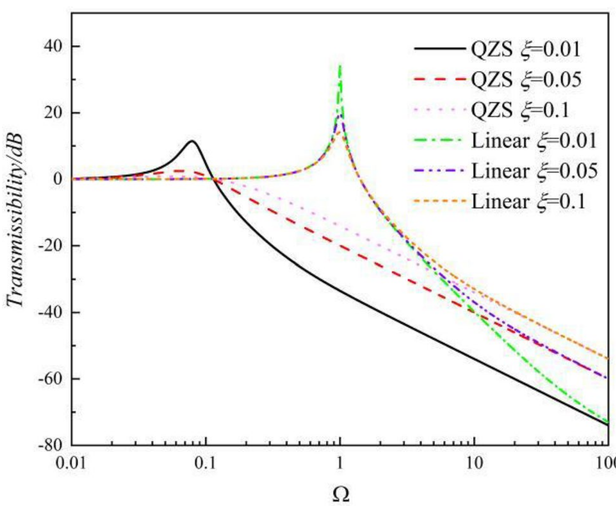

Fig. 16 Transmittance of linear vibration isolator and S_1 structure

It can be seen that the peak transmittance at the resonant frequency of the QZS superstructure corresponding to different damping coefficients is smaller than that of the linear isolator. In addition to the peak transmittance, the transmittance of the QZS element structure is also much smaller than that of the linear isolator for vibration frequencies located in the effective isolation range until the vibration frequency approaches a very large value, such as $\Omega = 100$.

For example, for the same damping factor $\xi = 0.01$ at vibration frequency ratio $\Omega = 3$, the transmittance of a linear vibration isolator is − 18.04 dB, S_1 is − 43.6 dB and S_2 is − 43.46 dB.

Effect of Damping Coefficient

As shown in Fig. 16 and Fig. 17, the damping coefficient does no effect on the effective isolation range of the QZS element structure and the linear vibration isolator, but the transmittance at different vibration frequencies is affected by the damping coefficient. For the QZS element structure and linear vibration isolators, the transmittance decreases with increasing damping coefficient when the vibration frequency is not in the effective vibration isolation range. However, when the vibration frequency is in the effective vibration isolation range, the transmittance increases as the damping coefficient increases. By comparing the QZS element structure with the linear vibration isolator, it is found that the damping coefficient has a greater effect on the QZS element structure than the linear vibration isolator in the effective vibration isolation range. The results show that the QZS structure with a smaller damping coefficient has better vibration isolation performance. Although purely from the point of view of vibration isolation, the increase in damping coefficient will reduce the vibration isolation effect, in the actual working process of the machine, the external excitation, in addition to

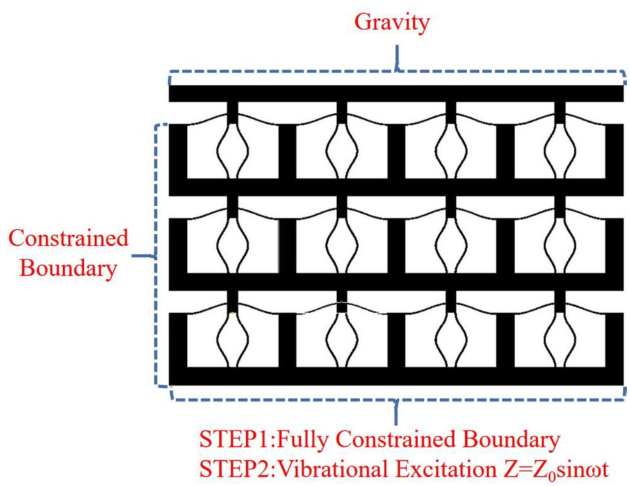

Fig. 18 Finite element model of S_1 vibration isolation simulation

simple harmonic vibration may also contain some irregular shocks. As the shock will cause the equipment larger amplitude of free vibration, the purpose of increasing the damping is to make the free vibration disappear quickly. Especially when the vibration isolation object through the resonance area, damping becomes more important. Therefore, in practical application, it is necessary to choose the appropriate damping coefficient for vibration isolation according to its situation.

Simulation of Vibration Isolation of QZS Structure

The finite element model containing the gravity of the object and the meta-structure S_1 is given in Fig. 18. The whole simulation process is divided into two steps. In the first step, the meta-structure is compressed under gravity when the bottom surface of the meta-structure is fully constrained, and this step will bring the meta-structure into the quasi-zero stiffness region. In the second step, the bottom surface is transformed from fully constrained to displacement-controlled vibration excitation. Since the transmittance in both Fig. 16 and Fig. 17 is derived from the CB condition, the boundary conditions on the left and right sides of the meta-structure are defined as CB throughout the simulation. The vibration excitation amplitude Z_0 is set to 5 mm. Three different excitation frequencies of S_1 and S_2 in the effective vibration isolation range were selected as $\Omega = 0.5$, $\Omega = 1$ and $\Omega = 2$. Then, the bottom and top displacements of the meta-structure were recorded to evaluate the vibration isolation performance corresponding to different vibration frequencies and damping coefficients.

The displacements at the bottom and top of the QZS element structure for S_1 and S_2 at different vibration frequencies and damping coefficients are shown in Figs. 19 and 20. The simulation results in Fig. 19 and Fig. 20 visualize the vibration isolation performance of the meta- structure. A significant reduction in amplitude was obtained through the meta-structure. It can also be seen that at the same vibration excitation frequency, the material with a smaller damping coefficient can obtain better vibration isolation performance, but the material with a smaller damping coefficient also takes a relatively long time to reach a smooth trend in amplitude. The main reason is that the smaller damping coefficient is weaker for the peak amplitude suppression, which makes it slower to reach the smooth state. For materials with the same damping coefficient, the vibration isolation performance of the meta-structure is better at higher vibration excitation frequencies. It can also be seen by the theoretical solution, i.e., Figs. 16 and 17, that the larger the frequency ratio, the smaller the transmittance at the same damping factor.

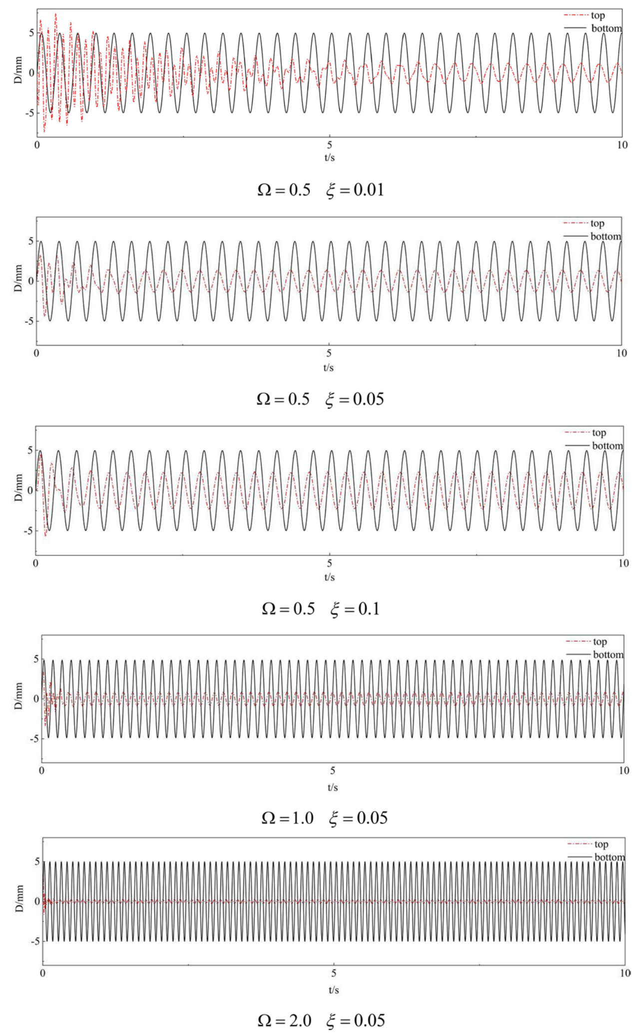

Fig. 19 Displacement at the bottom and top of the S_1 quasi-zero stiffness structure

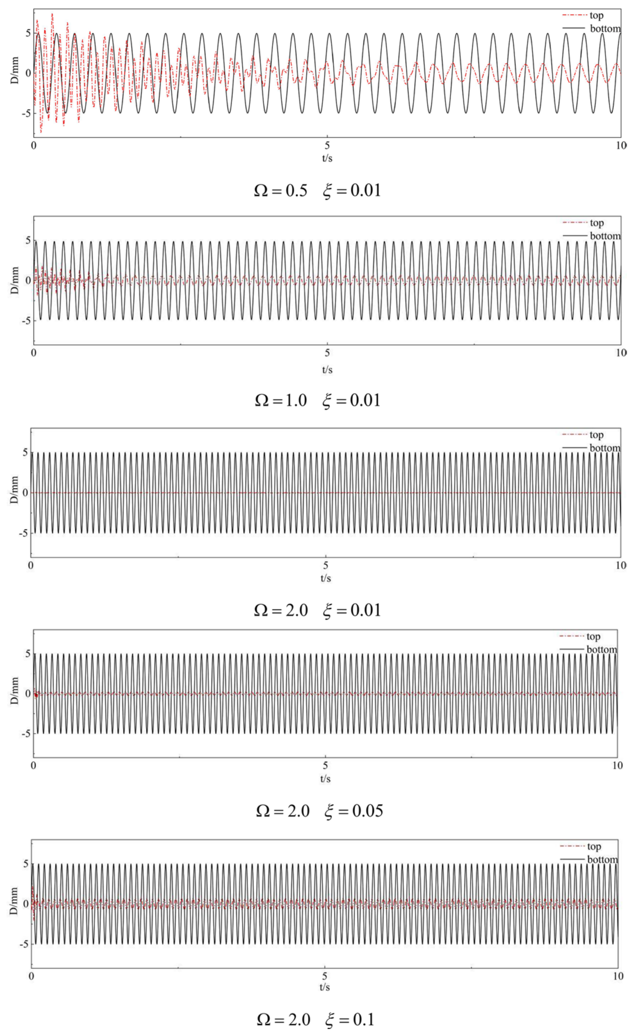

Fig. 20 Displacement at the bottom and top of the S_2 quasi-zero stiffness structure

That is, the further away from the peak frequency ratio of the system, the better the performance of the vibration isolation system. For each curve in Fig. 19 and Fig. 20, when the behavior of the meta-structure tends to be stable, the vibration amplitude obtained is Z_1, and Z_1 is much smaller than Z. It can be seen that the QZS meta-structure proposed in this paper has good vibration isolation performance. It also verifies that the theoretical results are accurate.

Conclusion

A meta-structural vibration isolation system with quasi-zero stiffness is designed based on the bionic human structure. Combining theoretical and simulation methods, the static and dynamic properties of this meta-structure are investigated. The vibration isolation performance of the proposed meta-structure was evaluated. The results show that the proposed QZS superstructure has good vibration isolation performance. To summarize the main research content of this paper, the following conclusions are drawn.

(1) A unit structure with quasi-zero stiffness characteristics can be realized through the rational design of horizontal cosine beams and vertical cosine beams. Based on the assumption of small deformation, the theoretical values of the mechanical properties of the meta-structure composed of numerous unit structures are derived.
(2) Static compression simulations of the unit structure and the meta-structure model were performed, and the results showed that the designed meta-structure has ideal quasi-zero stiffness characteristics, which are consistent with the theoretical results. Compared with the constrained boundary conditions, the free boundary conditions at the left and right boundaries of the meta-structure have an adverse effect on its quasi-zero stiffness characteristics. However, this effect gradually becomes smaller with the gradual increase of the number of unit cells.
(3) The dynamics analysis and the calculated transmittance are obtained that the meta-structure can obtain a larger vibration isolation range and lower transmittance compared with the linear vibration isolator. The peak value is also lower than that of the linear vibration isolator at the same damping factor. The proposed meta-structure has good vibration isolation performance.
(4) Theoretically, in the effective vibration isolation range, the peak vibration isolation rate decreases with the increase of the damping coefficient, and after the peak, the smaller the damping coefficient, the better the vibration isolation performance of the QZS structure. Simulation results of the vibration isolation performance of this element structure show that the element structure significantly reduces the vibration amplitude of the vibration isolation object. At higher vibration excitation frequencies, the smaller the damping coefficient, the better the vibration isolation performance of the meta-structure. In practical application, the vibration isolation system should be selected reasonably according to its situation for use.

The structural unit designed in this paper is a basic structure, and the mechanical properties achieved depend mainly on its own structure, which can be realized by different materials. In the future, more complex two-dimensional, three-dimensional and programmable vibration isolation element structures can be designed on this basis, which have greater application value.

Acknowledgements This work was supported by the Ye Qisun Science Foundation of National Natural Science Foundation of China (U2141231).

Author Contributions LM and LZ initiated this study and proposed the design of this work; HL designed the structure, performed research, derived the modeling and wrote the manuscript; JW and YW assist with design. All authors read and approved the final manuscript.

Data Availability Data sets supporting the conclusions of this paper are included in the article.

Declarations

Conflict of Interest The authors declare that they have no known competing financial interests or personal relationships that could have appeared to influence the work reported in this paper.

References

1. Dai HH, Jing XJ, Wang Y, Yue XK, Yuan JP (2018) Post-capture vibration suppress-ion of spacecraft via a bio-inspired isolation system. Mech Syst Signal Pr 105:214–240. https://doi.org/10.1016/j.ymssp.2017.12.015
2. Smith MC (1995) Achievable dynamic response of active suspensions in bounce and roll. Vehicle Syst Dyn 24(1):1–33. https://doi.org/10.1016/S1474-6670(17)45676-X
3. Kamesh D, Pandiyan R, Ghosal A (2012) Passive vibration isolation of reaction wheel disturbances using a low frequency flexible space platform. J Sound Vib 331(6):1310–1330. https://doi.org/10.1016/j.jsv.2011.10.033
4. He KD, Li Q, Liu L, Yang HJ (2021) Active vibration isolation of ultra-stable optical reference cavity of space optical clock. Aerosp Sci Technol 112:106633. https://doi.org/10.1016/j.ast.2021.106633
5. Li L, Wang L, Yuan L, Zheng R, Zhong J (2020) Micro-vibration suppression methods and key technologies for high-precision space optical instruments. Acta Astronaut 180:417–428. https://doi.org/10.1016/j.actaastro.2020.12.054
6. Wu Z, Jing X, Sun B, Li F (2016) A 6DOF passive vibration isolator using x-shapesupporting structures. J Sound Vib 380:90–111. https://doi.org/10.1016/j.jsv.2016.06.004
7. Kwon SC, Jo MS, Ko DH, Oh HU (2019) Viscoelastic multilayered blade-type passive vibration isolation system for a spaceborne cryogenic cooler. Cryogenics 105:102982. https://doi.org/10.1016/j.cryogenics.2019.102982
8. Lee JH, Dong YL, Lee MG (2011) Passive vibration reduction with silicone springs and dynamic absorber. Phys Procedia 19:431–435. https://doi.org/10.1016/j.phpro.2011.06.188
9. Niu MQ, Chen LQ (2022) Analysis of a bio-inspired vibration isolator with a compliant limb-like structure. Mech Syst Signal Pr 179:109348. https://doi.org/10.1016/j.ymssp.2022.109348
10. Feng X, Jing XJ (2019) Human body inspired vibration isolation: beneficial nonlinear stiffness, nonlinear damping & nonlinear inertia. Mech Syst Signal Pr 117:786–812. https://doi.org/10.1016/j.ymssp.2018.08.040
11. Molyneux WG (1957) Supports for Vibration Isolation. Her Majesty's Stationery Office, London
12. Tan XJ, Wang B, Chen S, Zhu SW, Sun YG (2019) A novel cylindrical negative stiffness structure for shock isolation. Compos Struct 214:397–405. https://doi.org/10.1016/j.compstruct.2019.02.030
13. Zhu SW, Wang B, Chen LM, Tan XJ, Ma L (2022) Enhance the energy dissipation ability of sleeve-type negative stiffness structures via a phase-difference mechanism. Int J Mech Sci 213:106803. https://doi.org/10.1016/j.ijmecsci.2021.106803
14. Zhou ZH, Dai ZH, Liu ZQ, Liu X, Chen SH, Li ZH, Zhou MR (2022) An adjustable low frequency vibration isolation with high-static-stiffness low-dynamic-stiffness property using a novel negative stiffness element. Appl Acoust 188:108571. https://doi.org/10.1016/j.apacoust.2021.108571
15. Huang XC, Liu XT, Sun JY, Zhang ZY, Hua HX (2014) Vibration isolation characteristics of a nonlinear isolator using Euler buckled beam as negative stiffness corrector: a theoretical and experimental study. J Sound Vib 333(4):1132–1148. https://doi.org/10.1016/j.jsv.2013.10.026
16. Gholikord M, Etemadi E, Imani M, Hosseinabadi M, Hu H (2022) Design and analysis of novel negative stiffness structures with significant energy absorption. Thin Wall Struct 181:110137. https://doi.org/10.1016/j.tws.2022.110137
17. Cao QJ, Wiercigroch M, Pavlovskaia EE, Grebogi C, Thompson JMT (2006) Archetypal oscillator for smooth and discontinuous dynamics. Phys Rev E 74(4):046218. https://doi.org/10.1103/PhysRevE.74.046218
18. Zhu GN, Cao QJ, Wang ZK, Zhang YT, Chen YS, Woo KC (2022) Road to entire insulation for resonances from a forced mechanical system. Sci Rep 12(1):21167. https://doi.org/10.1038/s41598-022-25691-4
19. Hao ZF, Cao QJ (2014) A novel dynamical model for GVT nonlinear supporting system with stable-quasi-zero-stiffness. J Theor App Mech 52(1):199–213
20. Sun XT, Jing XJ, Xu J, Cheng L (2014) Vibration isolation via a scissor-like structured platform. J Sound Vib 333(9):2404–2420. https://doi.org/10.1016/j.jsv.2013.12.025
21. Zhou XH, Zhao DX, Sun X, Yang X, Zhang JH, Ni T, Tang KH (2022) An asymmetric quasi-zero stiffness vibration isolator with long stroke and large bearing capacity. Nonlinear Dynam 108(3):1903–1930. https://doi.org/10.1007/s11071-022-07300-1
22. Chang YP, Zhou JX, Wang K, Xu DL (2021) A quasi-zero-stiffness dynamic vibration absorber. J Sound Vib 494:115859. https://doi.org/10.1016/j.jsv.2020.115859
23. Ye K, Ji JC, Brown T (2021) A novel integrated quasi-zero stiffness vibration isolator for coupled translational and rotational vibrations. Mech Syst Signal Pr 149:107340. https://doi.org/10.1016/j.ymssp.2020.107340
24. Xiong YH, Li FM, Wang Y (2022) A nonlinear quasi-zero-stiffness vibration isolation system with additional X-shaped structure: theory and experiment. Mech Syst Signal Pr 177:109208. https://doi.org/10.1016/j.ymssp.2022.109208
25. Hao ZF, Cao QJ (2015) The isolation characteristics of an archetypal dynamical model with stable-quasi-zero-stiffness. J Sound Vib 340:61–79. https://doi.org/10.1016/j.jsv.2014.11.038
26. Yan B, Yu N, Wang ZH, Wu CAY, Wang S, Zhang WM (2022) Lever-type quasi-zero stiffness vibration isolator with magnetic spring. J Sound Vib 527:116865. https://doi.org/10.1016/j.jsv.2022.116865
27. Lu ZQ, Liu WH, Ding H, Chen LQ (2022) Energy transfer of an axially loaded beam with a parallel-coupled nonlinear vibration isolator. J Vib Acoust 144(5):051009. https://doi.org/10.1115/1.4054324
28. Hao RB, Lu ZQ, Ding H, Chen LQ (2022) A nonlinear vibration isolator supported on a flexible plate: analysis and experiment.

Nonlinear Dynam 108(2):941–958. https://doi.org/10.1007/s11071-022-07243-7
29. Cai L, Liu W, Zhou M, Yan RS, Wang JG, Fan YD (2022) Research on lightning impulse voltage discharge characteristics of electromagnetic metamaterials. J Electrostat 116:103696. https://doi.org/10.1016/j.elstat.2022.103696
30. Xu XC, Xu RJ, Lin YS (2021) Tunable terahertz double split-ring metamaterial with polarization-sensitive characteristic. Opt Laser Technol 141:107103. https://doi.org/10.1016/j.optlastec.2021.107103
31. Cai XD, Tang R, Zhou HY, Li QS, Ma SJ, Wang DY, Liu T, Ling XH, Tan W, He Q, Xiao SY, Zhou L (2021) Dynamically controlling terahertz wavefronts with cascaded metasurfaces. Adv Photonics 3(3):036003. https://doi.org/10.1117/1.AP.3.3.036003
32. Li QS, Cai XD, Liu T, Jia M, Wu Q, Zhou HY, Liu HH, Wang QQ, Ling XH, Chen C, Ding F, He Q, Zhang YB, Xiao SY, Zhou L (2022) Gate-tuned graphene meta-devices for dynamically controlling terahertz wavefronts. Nanophotonics 11(9):2085–2096. https://doi.org/10.1515/nanoph-2021-0801
33. Zhang Y, He Y, Wang HW, Sun L, Su YK (2021) Ultra-broadband mode size converter using on-chip metamaterial-based luneburg lens. ACS Photonics 8(1):202–208. https://doi.org/10.1021/acsphotonics.0c01269
34. Gao NS, Zhang ZC, Deng J, Guo XY, Cheng BZ, Hou H (2022) Acoustic metamaterials for noise reduction: a review. Adv Mater Technol 7(6):2100698. https://doi.org/10.1002/admt.202100698
35. Lu CX, Hsieh MT, Huang ZF, Zhang C, Lin YJ, Shen Q, Chen F, Zhang LM (2022) Architectural design and additive manufacturing of mechanical metamaterials: a review. Engineering 17:44–63. https://doi.org/10.1016/j.eng.2021.12.023
36. Cai CQ, Zhou JX, Wang K, Xu DL, Wen GL (2022) Metamaterial plate with compliant quasi-zero-stiffness resonators for ultra-low-frequency band gap. J Sound Vib 540:117297. https://doi.org/10.1016/j.jsv.2022.117297
37. Li H, Zhao FG, Zhou XB (2019) A quasi-zero stiffness vibration isolator based on hybrid bistable composite laminate. LixueXuebao/Chin J Theor Appl Mech 51(2):354–363. https://doi.org/10.6052/0459-1879-18-266
38. Lin QD, Zhou JX, Wang K, Xu DL, Wen GL, Wang Q, Cai CQ (2022) Low-frequency locally resonant band gap of the two-dimensional quasi-zero-stiffness meta-materials. Int J Mech Sci 222:107230. https://doi.org/10.1016/j.ijmecsci.2022.107230
39. Ye K, Ji JC (2021) An origami inspired quasi-zero stiffness vibration isolator using a novel truss-spring based stack Miura-ori structure. Mech Syst Signal Pr 165:108383. https://doi.org/10.1016/j.ymssp.2021.108383
40. Fan HG, Yang LJ, Tian YC, Wang ZW (2020) Design of metastructures with quasi-zero dynamic stiffness for vibration isolation. Compos Struct 243:112244. https://doi.org/10.1016/j.compstruct.2020.112244
41. Matsumoto Y, Griffin MJ (1998) Dynamic response of the standing human body exposed to vertical vibration: influence of posture and vibration magnitude. J Sound Vib 212(1):85–107. https://doi.org/10.1006/jsvi.1997.1376
42. Smeathers JE (1989) Measurement of transmissibility for the human spine during walking and running. Clin Biomech 4(1):34–40. https://doi.org/10.1016/0268-0033(89)90065-X
43. Paddan GS, Griffin MJ (1993) Thetransmission of translational floor vibration to the heads of standing subjects. J Sound Vib 160(3):503–521. https://doi.org/10.1006/jsvi.1993.1041
44. Coermann RR (1962) The mechanical impedance of the human body in sitting and standing position at low frequencies. Hum Factors 4(5):227–253. https://doi.org/10.1177/001872086200400502
45. Qiu J, Lang JH, Slocum AH (2004) A curved-beam bistable mechanism. J Microelectromech Syst 13(2):137–146. https://doi.org/10.1109/JMEMS.2004.825308
46. Qiao C, Chen YL, Wang ST, Yang KJ, Qiu XM (2017) Theoretical analysis on the collapse of dumbbell-shaped tubes. Int J Mech Sci 123:20–33. https://doi.org/10.1016/j.ijmecsci.2017.01.031
47. Zhang Q, Guo DK, Hu GK (2021) Tailored mechanical metamaterials with programmable quasi-zero-stiffness features for full-band vibration isolation. Adv Funct Mater 31(33):2101428. https://doi.org/10.1002/adfm.202101428
48. Wang K, Zhou JX, Xu DL (2017) Sensitivity analysis of parametric errors on the performance of a torsion quasi-zero-stiffness vibration isolator. Int J Mech Sci 134:336–346. https://doi.org/10.1016/j.ijmecsci.2017.10.026
49. Liu SG, Feng LF, Zhao D, Shi XX, Zhang YP, Jiang JX, Zhao YC, Zhang CJ, Chen L (2019) A real-time controllable electromagnetic vibration isolator based on magnetorheological elastomer with quasi-zero stiffness characteristic. Smart Mater Struct 28(8):085037. https://doi.org/10.1088/1361-665X/ab2e44